A matter of delivery: nanocarriers and the engineering of protective immunity in tuberculosis vaccination

Szachniewicz, M.M.

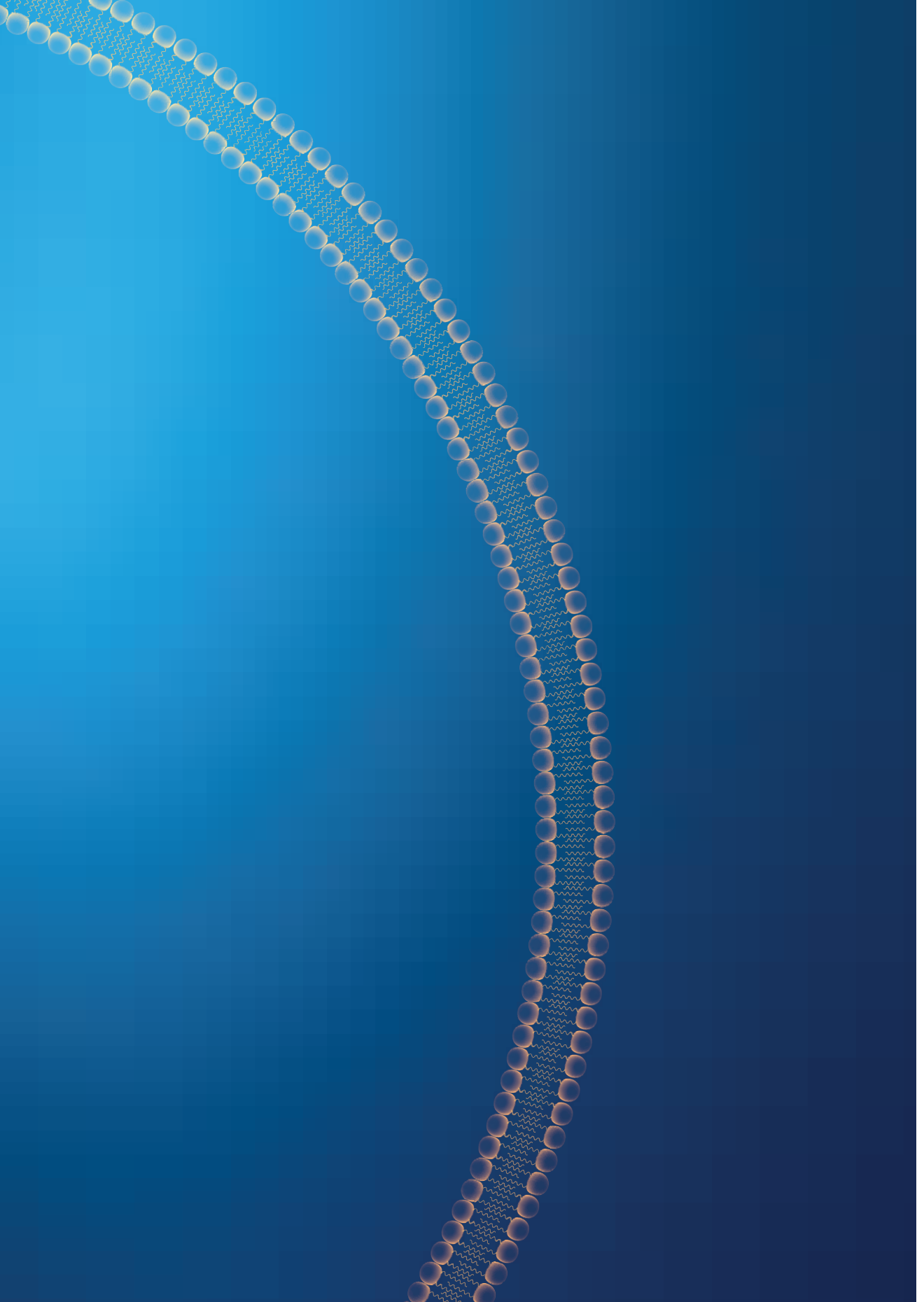

CHAPTER 6

Intradermal Versus Subcutaneous Immunization: Effects of Administration Route using a Lipid-PLGA Hybrid Nanoparticle Tuberculosis Vaccine

M.M. Szachniewicz, S.J.F. van den Eeden, K.E. van Meijgaarden, K.L.M.C. Franken, S. van Veen, A. Geluk, J.A. Bouwstra, T.H.M. Ottenhoff

Adapted from European Journal of Pharmaceutical Sciences, 2025, 205: 106995

ABSTRACT

Tuberculosis (TB) remains a significant global health challenge, latently affecting around a quarter of the global population. The sole licensed TB vaccine, *Mycobacterium bovis* Bacillus Calmette-Guérin (BCG), shows variable efficacy, particularly among adolescents and adults, underscoring the pressing need for more effective vaccination strategies. The administration route is crucial for vaccine efficacy, and administration via the skin, being rich in immune cells, may offer advantages over conventional subcutaneous routes, which lack direct access to abundant antigen-presenting cells.

This study compared the immunogenic effects of intradermal versus subcutaneous administration of a candidate TB vaccine delivering a Ag85B-ESAT6-Rv2034 (AER) multiphase fusion recombinant protein, in lipid-poly(D,L-lactic-co-glycolic acid) (lipid-PLGA) nanoparticles in mice. In-depth evaluation of immune responses in splenocytes was performed using 27-marker spectral flow cytometry. Both routes elicited significant T-cell responses. However, intradermal administration uniquely increased polyfunctional $CD4^+$ and $CD8^+$ T-cells producing IL-2, IFNγ, and TNFα, associated with protection against TB. Additionally, it significantly increased $CD69^+$ B-cell counts and induced higher AER-specific antibody titers, particularly IgG2a. These results underscore the superior immunogenic potential of intradermal vaccine administration by effectively inducing immune cells associated with TB protection, highlighting its significance in the development of new vaccine strategies.

1. INTRODUCTION

Tuberculosis (TB), caused by the bacterium *Mycobacterium tuberculosis* (Mtb), is one of humanity's oldest and deadliest infectious diseases.[1] It remains a major global health problem, primarily affecting the lungs but capable of impacting other body systems. TB is widespread globally, especially in low-middle income countries and in marginalized communities.[2] It is estimated that about a quarter of the entire human population is latently infected with Mtb. Despite advances in medicine, TB continues to pose a significant threat, aggravated by factors such as inadequate healthcare systems, social inequality, concurrent type-2 diabetes and co-infection with HIV/AIDS.[1] In 2021, 10.6 million people fell ill, and 1.6 million people died because of TB.[3] These statistics highlight the urgent need for improved public health strategies, increased awareness, and access to effective treatment and prevention measures such as vaccines.

The Bacillus Calmette-Guérin (BCG) vaccine, derived from *Mycobacterium bovis*, is currently the only licensed vaccine for TB. Its efficacy against pulmonary TB in adults and adolescents varies substantially, ranging from 0 to 80 %.[4] Yet, it remains extensively utilized due to its proven effectiveness in preventing various forms of TB in children.[5]

Subunit vaccines, formulated using synthesized or purified antigens, DNA, or RNA, are noted for their safety and broad applicability, including for individuals with weakened immune systems.[6] Despite their safety profile, these vaccines often face challenges in terms of immunogenicity, highlighting the need for enhanced delivery strategies.[7] To address this, the study described here focuses on using biocompatible nanoparticles (NPs) in vaccine delivery. These NPs are designed to protect antigens from degradation and premature elimination. Simultaneous encapsulation of antigens and adjuvants may improve the uptake efficacy by antigen-presenting cells (APCs).

In preclinical vaccine delivery research, lipid-PLGA hybrid NPs have emerged as highly effective nanostructures, as evidenced in various studies.[8–13] These NPs are engineered with a biodegradable poly(lactic-co-glycolic acid) (PLGA) core surrounded by a lipid layer. The hybrid nature of these NPs leverages the benefits of two commonly researched types of nanoparticles: PLGA NPs and liposomes. The

PLGA core provides a stable and solid structure for the prolonged and controlled release of antigens and adjuvants, while the lipid shell, often cationic, addresses PLGA's limited immunogenicity. This shell enhances uptake by antigen-presenting cells (APCs), slows down the degradation of the PLGA core by restricting water infiltration, and thus ensures a more controlled release of the cargo.[14–17] In vaccine development, these cationic lipid-PLGA hybrid NPs have shown promising results, significantly boosting immunogenicity and triggering both humoral and cellular immune responses.[11–13,18]

Alternative routes of vaccine administration may potentially further improve the effectiveness of vaccines. Intradermal vaccination is an alternative to intramuscular and subcutaneous routes and offers several advantages. The skin is easily accessible, and, in contrast to muscle and subcutaneous (s.c.) tissues, contains many immune cells, especially APCs such as dendritic cells and Langerhans cells.[19,20] Intradermal immunization was shown to be as effective as the conventional immunization schemes but at lower doses, thus reducing costs and sparing antigen.[21–24] Another advantage is that intradermal (i.d.) injections allow for the possibility of vaccinating less painfully compared to intramuscular and s.c. injections, which may translate to better compliance, especially in children.[25]

This study explored the effect of the administration route (s.c. vs. i.d.) in mice on the immunogenicity of a candidate TB vaccine. The fusion protein antigen, Ag85B-ESAT6-Rv2034 (AER), combined with adjuvants like monophosphoryl lipid A (MPLA) and cytosine-phosphate-guanine motifs oligodeoxynucleotides (CpG ODN) was used in the formulation. This vaccine was delivered using pH-sensitive lipid-PLGA hybrid NPs. The AER antigen is a fusion of three proteins: Ag85B, an epitope-rich immunodominant Mtb antigen;[26] ESAT6, a potent immunomodulatory antigen not expressed by BCG;[27,28] and Rv2034, a potent antigen expressed by Mtb *in vivo*.[29] Murine immune responses were assessed using a 27-marker spectral flow cytometry, focusing on $CD4^+$, $CD8^+$ T-cell, and B-cell responses. Additionally, serum antigen-specific antibody levels were measured.

2. MATERIALS AND METHODS

2.1 Materials

The phospholipids 1,2-dioleoyl-sn-glycero-3-phosphocholine (DOPC), 1,2-dioleoyl-sn-glycero-3-ethylphosphocholine chloride salt (EPC), 1,2-dioleoyl-sn-glycero-3-phosphoethanolamine (DOPE), monophosphoryl lipid A (PHAD), synthetic (MPLA), and N-(4-carboxybenzyl)-N,N-dimethyl-2,3-bis(oleoyloxy)propan-1-aminium (DOBAQ) were procured from Avanti Polar Lipids, Inc., (USA). Class B CpG oligonucleotide ODN1826 was purchased from InvivoGen (the Netherlands). Poly(lactic-co-glycolic acid) (PLGA) (acid terminated), a copolymer ratio of lactide to glycolide of 50:50, and a molecular weight range of 24,000 to 38,000 was acquired from Merck Chemicals B.V. (the Netherlands). Hardware for microfluidic connections, including interconnect tees compatible with capillaries of 360 µm (outer diameter), one-piece (for 360 µm capillaries and for 1/16" tubings), and two-piece fittings (360- µm-to-1.6-mm and 1.6-mm-to-360- µm) for capillaries and tubings of specified dimensions, along with Luer-lock adapters (for use with 360 µm capillaries and 1/16" tubings), were supplied by Mengel Engineering (Denmark). Capillary tubing made of polyether ether ketone (PEEK) (inner diameter of 0.02" and outer diameter of 1/16") as well as a Teflon tube (1/16"), were sourced from Fisher Emergo B.V. and Waters Chromatography B.V., respectively (the Netherlands). Standard polyimide-coated fused silica tubing of 75 µm and 250 µm inner diameters and an external diameter of 360 µm was obtained from BGB Analytik Benelux B.V. (the Netherlands). Polytetrafluoroethylene (PTFE) Luer-lock Hamilton gastight syringes of varying volumes (1710TLL 100 µL, 1001TLL 1 ml, and 1010TLL 10 ml) were purchased from Merck (Germany).

The recombinant fusion protein AER was prepared following the protocol outlined by Franken et al.[30] The genetic material from the Mycobacterium tuberculosis (Mtb) laboratory strain H37Rv was amplified via polymerase chain reaction (PCR) utilizing genomic DNA as the template. The resulting gene products were subsequently cloned into a bacterial vector (*Escherichia coli* strain BL21 DE3) employing an N-terminal hexahistidine (His) tag via Gateway technology (Invitrogen, USA), with sequencing confirming the accuracy of the insertions. Produced AER was subsequently purified as described previously.[30] AER is a 519-amino acid protein with a molecular mass of 56.13 kDa, an isoelectric point (pI) of 5.60, and an aliphatic index of 73.64. The protein

quality was evaluated using gel electrophoresis, Coomassie brilliant blue staining, and Western blot analysis using an anti-His antibody (Invitrogen, USA) to confirm protein size and purity was found to be >95 %. The ToxinSensor Chromogenic Limulus Amebocyte Lysate (LAL) Endotoxin Assay Kit (GenScript, USA) was utilized to quantify endotoxin levels within the protein preparation, confirming contamination levels were below 5 endotoxin units per milligram of protein. Cellular toxicity and non-specific T-cell activation were assessed and excluded using in vitro assays with human peripheral blood mononuclear cells (non-responsive to stimulation with purified protein derivative (PPD) of Mtb) obtained from healthy Dutch donors (recruited at the Sanquin Blood Bank, Leiden, the Netherlands).

2.2 Production of lipid-PLGA hybrid NPs

Lipid-PLGA hybrid NPs were produced by employing a previously described modular microfluidic system.[31] This system utilized a four-component approach (Figure 1). In brief, two flows from Syringe 1 (PLGA in acetonitrile) and Syringe 2 (AER/CpG in water for injection) were combined at a T-junction, creating a T-flow. This mixture was subsequently combined with a flow from Syringe 3 (water for injection) at a subsequent junction, forming a co-flow arrangement where the merged stream from Syringes 1 and 2 served as the inner flow, and the stream from Syringe 3 acted as the outer flow. The flow from this assembly was directed into another T-junction, where it was combined with a lipid mixture consisting of DOPC:DOPE:DOBAQ:EPC in molar ratio 3:5:2:4 (the optimization of the lipid formulation was described previously[32]) and MPLA (in ethanol) from Syringe 4. The flow rates were precisely controlled, with Syringe 1, 2, 3, and 4 delivering fluids at 37.5, 1250, 3712, and 1250 µl/min, respectively, achieving a cumulative flow rate of 6249.5 µl/min. Three different batches were prepared for each immunization, as explained in section *2.5 Immunizations*. The contents of the syringes are summarized in Table 1.

After production, the nanoparticle suspension underwent evaporation and was concentrated twofold for s.c. immunization and tenfold for i.d. immunizations under a stream of nitrogen to accommodate for different injection volume requirements. The volume was adjusted using water for injections and phosphate buffer (PB) concentrate so that the end PB concentration was 10 mM, and pH 7.4. The concentrations of constituents of the resulting suspensions are summarized in Table 2.

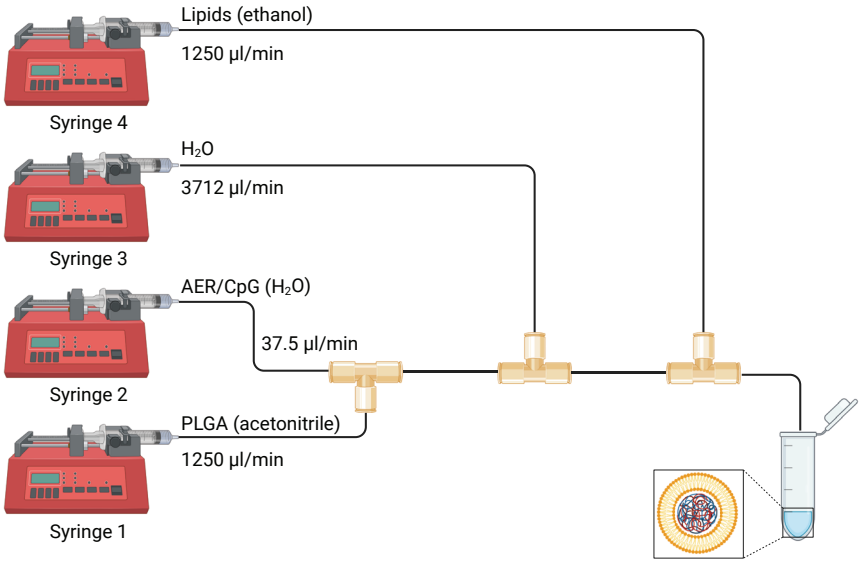

Figure 1. Schematic representation of microfluidic system used for the production of hybrid lipid-PLGA NPs. Syringes 1-4 contain PLGA, AER/CpG, H_2O, and lipids (DOPC:DOPE:DOBAQ:EPC 3:5:2:4 + MPLA), respectively. Solvents are indicated in parentheses as well as output flow rates. Created with BioRender.com.

Table 1. Summary of the concentrations of constituents in syringes 1-4 used in the microfluidic system for each immunization group. AER – Ag85B-ESAT6-Rv2034 protein, lipids -DOPC:DOPE:DOBAQ:EPC 3:5:2:4 (molar ratio).

Group	1) PLGA (mg/ml)	2) AER/CpG (mg/ml)	3) H_2O (mg/ml)	4) Lipids/MPLA (mg/ml)
2.5 µg s.c.	5.00	1.05/1.05	—	5.00/0.0125
0.5 µg i.d.	6.40	0.28/1.40	—	6.40/0.0170
2.5 µg i.d.	6.40	1.40/1.40	—	6.40/0.0170

Table 2. Summary of the end concentrations (after evaporation and volume adjustment) of constituents in each formulation. AER – Ag85B-ESAT6-Rv2034 protein, lipids -DOPC:DOPE:DOBAQ:EPC 3:5:2:4 (molar ratio).

Formulation	PLGA (mg/ml)	AER/CpG (mg/ml)	H_2O (mg/ml)	Lipids/MPLA (mg/ml)
2.5 µg s.c.	2000	12.5/12.5	—	2000/5
0.5 µg i.d.	13400	16.8/84.0	—	13400/34
2.5 µg i.d.	13400	84.0/84.0	—	13400/34

2.3 Physicochemical properties of NPs

The characterization of liposomal formulations, specifically their hydrodynamic diameter (Z-average size) and polydispersity index (PDI), was conducted through dynamic light scattering (DLS), while their zeta potential was assessed via laser Doppler electrophoresis as described previously.[33] Briefly, the NPs were diluted to 0.25 mg/mL lipid concentration in a 10 mM PB at a pH of 7.4 for these analyses. This solution was then transferred into 1.5 ml VWR Two-Sided Disposable Polystyrene (PS) Cuvettes (VWR, the Netherlands) for measurements. The evaluation was carried out in triplicate, using a minimum of ten individual runs at a controlled temperature of 20 °C, utilizing a Nano ZS Zetasizer equipped with a 633 nm laser and optics positioned at 173° (Malvern Instruments, UK). Data processing and analysis were performed using the Zetasizer Software version 7.13 (Malvern Instruments).

2.4 Mice

C57Bl/6 mice (stock number SC1300004) were supplied by The Jackson Laboratory (USA) and housed within the animal care facilities of Leiden University Medical Center (LUMC). Female mice aged 6 to 8 weeks and age-matched were selected for each experiment.

All mouse experiments were individually designed, reviewed, and ethically approved by the institutional Animal Welfare Body at the LUMC, and carried out under project license number AVD116002017856, issued by the Netherlands' authoritative body on animal experimentation, the CCD. These experiments strictly followed the Dutch Act on Animal Experimentation and the European Union Directive 2010/63/EU within the LUMC facility. Mice were housed in separately ventilated cages with no more than seven mice per cage, and experiments began only after a one-week acclimatization period following transport.

2.5 Immunizations

Mice received vaccinations utilizing pH-sensitive lipid-PLGA hybrid NPs as delivery systems for AER protein antigen and molecular adjuvants MPLA and CpG. Lipid-PLGA hybrid NPs consist of DOPC:DOPE:DOBAQ:EPC 3:5:2:4 (lipid layer) and PLGA (core). The vaccination protocol entailed administering three subcutaneous (s.c.) or intradermal (i.d.) injections. S.C. injections (200 µl) were performed in the right

flank, and i.d. injections (30 µl) in the tail base area. Immunizations were performed biweekly, using formulations as detailed in Table 3. Vaccine formulations were freshly prepared a day prior to each immunization and stored at 4 °C to ensure quality and consistency. Four weeks following the final vaccination, the mice were humanely euthanized with CO_2. The timeline of the experiment is summarized in Figure 2.

Table 3. Summary of vaccination groups and doses of vaccine constituents administered to a mouse in a single immunization. AER – Ag85B-ESAT6-Rv2034 protein, lipid -DOPC:DOPE:DOBAQ:EPC 3:5:2:4 (molar ratio).

Group	Route	AER (µg)	Lipid (µg)	PLGA (µg)	CpG (µg)	MPLA (µg)
Naïve	NA	NA	NA	NA	NA	NA
2.5 µg s.c.	subcutaneous	2.5	400	400	2.5	1
0.5 µg i.d.	intradermal	0.5	400	400	2.5	1
2.5 µg i.d.	intradermal	2.5	400	400	2.5	1

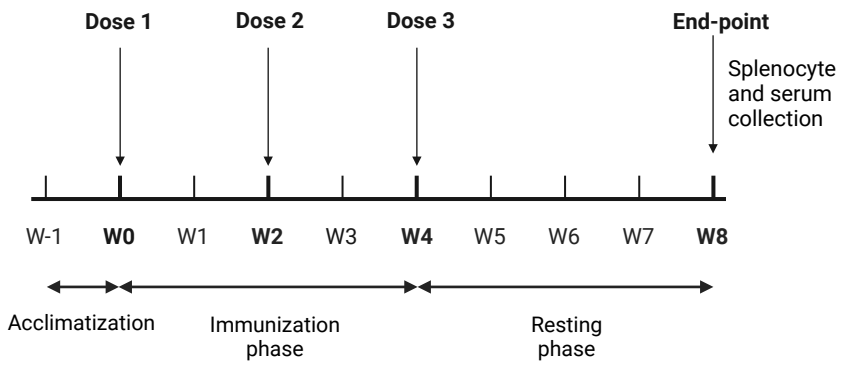

Figure 2. Overview of the immunization experiment timeline. Created with BioRender.com.

2.6 Splenocyte cultures

Splenocytes harvested from immunized mice were suspended at a density of 3×10^6 cells/ml in Iscove's Modified Dulbecco's Medium (IMDM; Lonza, Switzerland), supplemented with 2 mM GlutaMAX™ and 100 U/100 µg/ml of penicillin-streptomycin (both sourced from Gibco, Paisley, UK), along with 8 % heat-inactivated fetal bovine serum (FBS; Greiner, Frickenhausen, Germany). These cells were then restimulated *in vitro* using 5 µg/ml of AER at 37 °C / 5 % CO_2. Six days later, the splenocytes received a second stimulation with the identical antigen for 5 hours, followed by

adding 2.5 µg/ml Brefeldin A (Sigma, Merck, Darmstadt, Germany) and incubation overnight. Subsequently, these cells were harvested and used for flow cytometry analysis.

2.7 Antibody enzyme-linked immunosorbent assay (ELISA)

Blood samples were collected from immunized mice via cardiac puncture following humane euthanasia with CO_2 and were immediately placed on ice for preservation. Subsequent centrifugation at 15,000 rpm for 10 minutes facilitated the separation of sera. The presence of antibodies specific to proteins within the sera was quantified using ELISA, as described previously.[31,34,35] For this purpose, Microlon 96-well plates (Greiner Bio-One GmbH, Germany) were coated overnight at 4 °C with either AER (5 µg/ml) or a control solution of PBS / 0.4 % bovine serum albumin (BSA; Sigma, Merck, Darmstadt, Germany), followed by a blocking phase of 2 hours with PBS containing 1 % BSA and 1 % Tween-20. Serum samples were diluted to 100 µl per well using a series of serial dilutions starting at 1:200 and incubated at 37 °C for 2 hours. After washing with PBS/0.05 % Tween-20, the plates were incubated with horseradish peroxidase (HRP)-conjugated rabbit anti-mouse antibodies targeting total IgG, IgG1, and IgG2a (Dako, Denmark) for another 2 hours at 37 °C. After washing, 100 µl of tetramethylbenzidine (TMB; Merck, Germany) substrate was added to each well for 15 minutes. The reaction was halted by adding 1M H_2SO_4, and the optical density at 450 nm (OD450) was measured using a Spectramax i3x spectrometer (Molecular Devices, CA, USA).

2.8 Flow cytometry

The surface and intracellular staining methodology was detailed in prior publications.[31,35] The list of antibodies is summarized in Table 4. Briefly, splenocytes were transferred to 96-well plates and washed with PBS. The cells were stained using the Zombie UV Fixable Viability Kit (BioLegend, the Netherlands) at a dilution of 1:250 in PBS, with each well receiving 100 µl of the dye solution for 30 minutes. Subsequently, the cells were washed with FACS buffer (PBS supplemented with 0.1 % BSA). The cells were then blocked with 20 µl of 5 % normal mouse serum (Thermo Fisher Scientific Inc., Bleiswijk, the Netherlands) in FACS buffer, followed by additional washes before staining with CCR7 for 30 minutes at 37 °C. After another two washes, cells were incubated with 50 µl per well of an antibody mixture, which included

Table 4. List of antibodies used in for spectral flow cytometry analysis of $CD4^+$, $CD8^+$, and $CD3^-$ $CD19^+$ cells.

Marker	Fluorochrome	Clone	Manufacturer
CCR7 (CD197)	PE/Cyanine5	4B12	BioLegend
CD273	Brilliant Ultra Violet (BUV) 395	TY25	BD Biosciences
CD8b.2	BUV 496	53-5.8	BD Biosciences
CD80	BUV 661	16-10A1	BD Biosciences
CD69	BUV 737	H1.2F3	BD Biosciences
CD25	Brilliant Violet (BV) 480	PC61	BD Biosciences
CD154	Super Bright 436	MR1	Thermo Fisher
IgD	Pacific Blue	11-26c.2a	BioLegend
I-A/I-E (MHC class II)	BV 510	M5/114.15.2	BioLegend
CD44	BV 570	IM7	BioLegend
PD-1 (CD279)	BV 605	29F.1A12	BioLegend
CXCR3 (CD183)	BV 650	CXCR3-173	BioLegend
KLRG1 (MAFA)	BV 711	2F1/KLRG1	BioLegend
CCR6 (CD196)	BV 785	29-2L17	BioLegend
CD4	Spark Blue 550	GK1.5	BioLegend
CCR5 (CD195)	PerCP/Cyanine5.5	HM-CCR5	BioLegend
CD19	PE Fire 640	6D5	BioLegend
CD138	APC	281-2	BioLegend
B220 (CD45R)	Spark NIR 685	RA3-6B2	BioLegend
CD62L (L-selectin)	APC/Fire 750	MEL-14	BioLegend
CD3	APC/Fire 810	17A2	BioLegend
IL-2	APC-R700	JES6-5H4	BD Biosciences
IL-17A	PE	eBio17B7	Thermo Fisher
IgM	FITC	RMM-1	BioLegend
IL-10	PE/Dazzle 594	JES5-16E3	BioLegend
TNFα	PE/Cyanine7	MP6-XT22	BioLegend
IFNγ	Alexa Fluor 647	XMG1.2	BioLegend

10 µl per well of BD Horizon Brilliant Stain Buffer Plus (BD Biosciences, Belgium), for 30 minutes at 4 °C. Following two more washes with FACS buffer, cells were fixed and permeabilized using the eBioscience Foxp3/Transcription Factor Staining Buffer Set (Invitrogen, Thermo Fisher Scientific, Belgium) at 4 °C for an hour. After washing, intracellular staining was conducted with an antibody mix diluted in permeabilization buffer, with a 45-minute incubation in 50 µl per well of the antibody mixture. After two final washes in FACS buffer, cells were resuspended in 100 µl per well of FACS buffer and stored at 4 °C until analysis. The samples were analyzed using a Cytek Aurora spectral flow cytometer (Cytek Biosciences, Fremont, CA, USA) at the Flow Cytometry Core Facility of Leiden University Medical Center, the Netherlands.

2.9 Flow cytometry data analysis

Data was analyzed using FlowJo version 10.8.0 (FlowJo LLC, BD, USA) and OMIQ (www.omiq.ai) platforms. Initially, manual gating was performed in FlowJo to exclude debris, doublets, and cells affected by acquisition disturbances. Subsequent gating focused on the distinction between CD3 and CD19 markers, enabling the separation of T-cells ($CD3^+$ $CD19^-$) and B-cells ($CD3^-$ $CD19^+$), with each subgroup being exported with a minimum of 20,000 events into OMIQ for further analysis. Within OMIQ, the data underwent additional cleaning via FlowAI, followed by establishing single marker gates. Boolean gating techniques were then applied to derive combinations of gates. The counts derived from all Boolean gating were retrieved for further analysis, and statistical analysis was carried out.

2.10 Statistical analysis

With the Benjamini-Hochberg false discovery rate (FDR) adjustment, the Mann-Whitney U test was employed to discern differentially abundant cell populations, utilizing the R[36] and RStudio,[37] interface for analysis. For comparisons among vaccination cohorts, statistical assessments were executed in GraphPad Prism, version 8.01 (GraphPad Software, Prism, USA), using the Kruskal-Wallis test followed by Dunn's posthoc test without correction for multiple comparisons. This non-parametric test was used to evaluate differences across three or more groups in relation to a control group. A significance threshold was established at $P < 0.05$, with specific notation indicating levels of statistical significance: *$P < 0.05$, **$P < 0.01$, ***$P < 0.001$, ****$P < 0.0001$. Graphs show median ± interquartile range (IQR).

3. RESULTS

3.1 Characterization of lipid-PLGA hybrid NPs and study design

Lipid-PLGA hybrid NPs were used to deliver AER antigen with CpG and MPLA adjuvants. The produced NPs were characterized, and the results are summarized in Table 5. All the produced formulations had very similar physicochemical characteristics – size 145-155 nm, PDI 0.16, and Zeta-potential 25 mV. These results assure that the differences in immunological responses are unlikely to be caused by differences in the formulations. The day after the formulations were produced and characterized, the vaccines were administered to mice. Three immunizations were administered two weeks apart, with a fresh batch of vaccines prepared for each immunization. Any remaining vaccine from each batch was discarded. Two different routes of administration were tested: subcutaneous (s.c.) and intradermal (i.d.). The immunization groups are detailed in Table 3.

Table 5. Physicochemical properties of pH-sensitive lipid-PLGA hybrid NPs used for immunization of mice. Results represent an average of n = 6 batches (3 batches used in 2 experiments). Lipid-PLGA hybrid NPs consisting of AER, DOPC:DOPE:DOBAQ:EPC 3:5:2:4 (lipid layer) and PLGA (core).

Formulation	Z-average size (nm)	PDI (-)	Zeta-potential (mV)
2.5 µg/mouse AER s.c.	143.9 ± 18.5	0.16 ± 0.02	25.8 ± 1.1
2.5 µg/mouse AER i.d.	143.1 ± 18.5	0.16 ± 0.01	25.1 ± 2.8
0.5 µg/mouse AER i.d.	156.4 ± 14.7	0.17 ± 0.01	25.7 ± 0.6

3.2 AER-specific T-cell responses in splenocytes ex vivo

Splenocytes from immunized mice were harvested and restimulated with AER. Subsequently, splenocytes were stained and spectral flow cytometry was performed to evaluate immune responses. To investigate T-cell populations, uniform manifold approximation and projection (UMAP) was employed for dimensionality reduction and global qualitative analysis across experimental groups. UMAP analysis included all $CD3^+$ $CD19^-$ events to provide a comprehensive overview of T-cell distributions (Figure 3). Visual inspection of the UMAP plots revealed prominent variations

in T-cell abundance between experimental groups. Immunized groups showed increased abundance of several $CD4^+$ and $CD8^+$ T-cell subpopulations compared to the unimmunized control.

The color-gradient plots highlighted that many of the increased T-cell populations in the immunized groups expressed cytokines IL-2, TNFα, and IFNγ, as well as the surface marker CD62L, indicative of functional immune activation. Furthermore, a distinct difference in the abundance of $IFN\gamma^+$ $CD4^+$ and $IFN\gamma^+$ $CD8^+$ T-cells was observed when comparing the subcutaneous group (2.5 µg dose) with the intradermal group, suggesting route-dependent immune responses.

These qualitative findings prompted further analysis to identify differentially abundant T-cell subsets, which were subsequently subjected to quantitative univariate analysis to reveal the immune responses elicited in the experimental groups.

Criteria for selection included populations exceeding 100 events and possessing distinct phenotypic markers that not only set them apart from other subsets but also provided insights into their potential functional roles.

T-cells, especially $CD4^+$ T-cells, are crucial immune components in protection against Mtb infection.[38,39] The differential abundance analysis revealed several differentially abundant $CD4^+$ T-cell subsets (Figure 4). Notably, three distinct populations were observed that produced one, two, or three cytokines simultaneously. Two Th1 subsets were significantly increased in vaccinated mice compared to naïve mice: trifunctional $CD4^+$ $IL\text{-}2^+$ $IFN\gamma^+$ $TNF\alpha^+$ $IL\text{-}17A^-$ $IL\text{-}10^-$ $CD44^-$ $CD62L^+$ $CCR7^-$, and bifunctional $CD4^+$ $IL\text{-}2^+$ $IFN\gamma^+$ $TNF\alpha^-$ $IL\text{-}17A^-$ $IL\text{-}10^-$ $CD44^-$ $CD62L^+$ $CCR7^-$, both exhibiting central memory-like phenotypes. Trifunctional Th1 cells were increased only in mice vaccinated i.d. but not s.c. Moreover, mice vaccinated with 2.5 µg AER i.d. had significantly higher counts of the trifunctional Th1 cells compared to the corresponding group vaccinated s.c. It should be noted that although the data patterns were consistent, there was a substantial spread within the data from the two experiments. Interestingly, the highest cell counts in s.c. vaccinated mice were observed for a monofunctional subset of $CD4^+$ $IL\text{-}2^+$ $IFN\gamma^-$ $TNF\alpha^-$ $IL\text{-}17A^-$ $IL\text{-}10^-$ $CD44^-$ $CD62L^+$ $CCR7^-$ cells.No Th17 responses were observed. $CD4^+$ T-cell responses in lower and higher AER i.d. vaccinated groups were very similar.

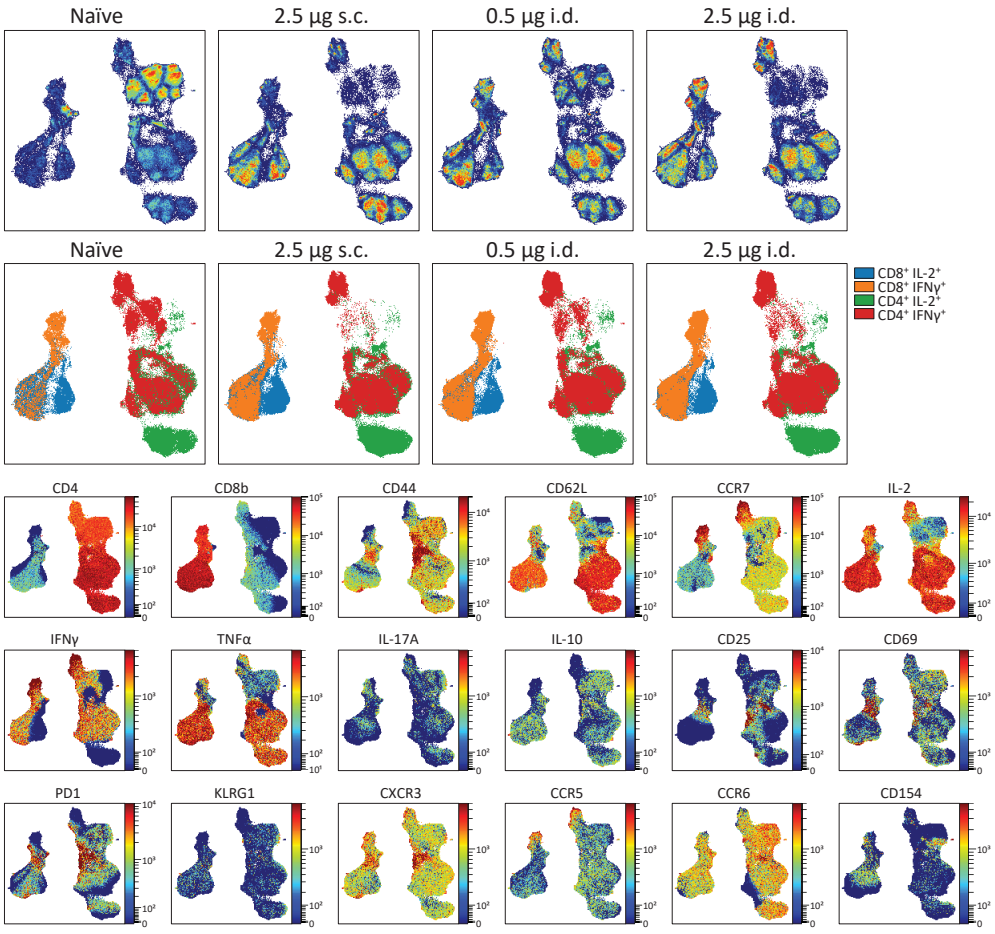

Figure 3. UMAP plots visualize dimensionally reduced phenotypes of spleen-derived $CD4^+$ and $CD8^+$ T-cells ($CD3^+$ $CD19^-$) from all tested mice in each group, demonstrating differences in cell population abundances. Additionally, color-continuous plots were employed to illustrate the distribution of phenotypical markers. Groups represent: naïve – unimmunized mice, 2.5 µg s.c. – immunization with 2.5 µg AER subcutaneously, 0.5 µg i.d. – immunization with 0.5 µg AER intradermally, 2.5 µg i.d. – immunization with 2.5 µg AER intradermally.

Similarly, differentially abundant $CD8^+$ T-cells were found (Figure 5), which play a role in chronic stages of Mtb infection. The largest group of $CD8^+$ T-cells identified in this study was a trifunctional type of central memory T-cells, characterized as$CD8^+$ $IL\text{-}2^+$ $IFN\gamma^+$ $TNF\alpha^+$ $IL\text{-}17A^-$ $IL\text{-}10^-$ $CD44^-$ $CD62L^+$ $CCR7^-$. This subset was significantly increased in all i.d. vaccinated groups, unlike those vaccinated s.c. Additionally,

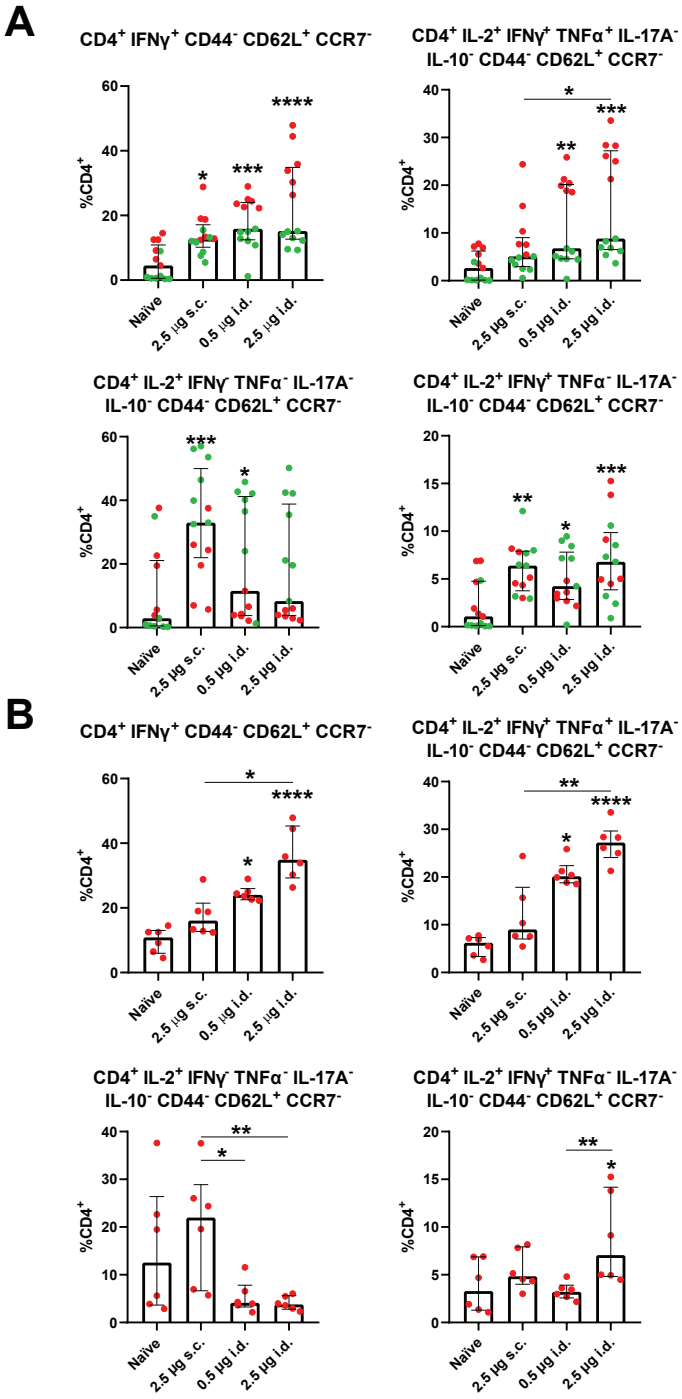
A
CD4+ IFNγ+ CD44- CD62L+ CCR7-
CD4+ IL-2+ IFNγ+ TNFα+ IL-17A- IL-10- CD44- CD62L+ CCR7-
CD4+ IL-2+ IFNγ- TNFα- IL-17A- IL-10- CD44- CD62L+ CCR7-
CD4+ IL-2+ IFNγ+ TNFα- IL-17A- IL-10- CD44- CD62L+ CCR7-
B
CD4+ IFNγ+ CD44- CD62L+ CCR7-
CD4+ IL-2+ IFNγ+ TNFα+ IL-17A- IL-10- CD44- CD62L+ CCR7-
CD4+ IL-2+ IFNγ- TNFα- IL-17A- IL-10- CD44- CD62L+ CCR7-
CD4+ IL-2+ IFNγ+ TNFα- IL-17A- IL-10- CD44- CD62L+ CCR7-
%CD4+
Naïve
2.5 µg s.c.
0.5 µg i.d.
2.5 µg i.d.

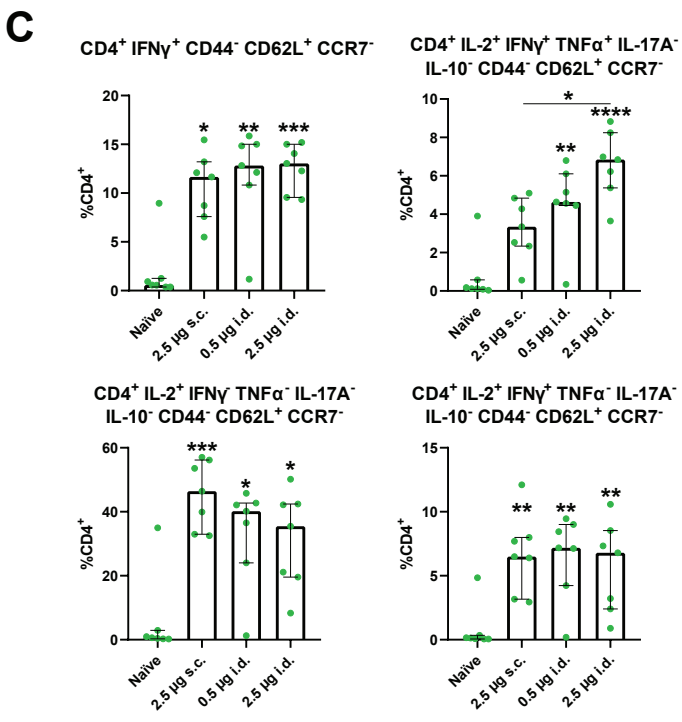

←↑ **Figure 4.** Variations in the abundance of CD4⁺ T-cell populations within restimulated splenocytes from immunized mice. Each graph identifies the markers characterizing the respective populations and displays the percentage values of these populations as median ± IQR within the CD3⁺ CD19⁻ CD4⁺ CD8⁻ cell subset. A) Combined results from both experiments. Each dot represents a single mouse, and the results of the same experiment are shown in one color. n = 13 (mice). B) Results from the first experiment. n = 6 (mice). C) Results from the second experiment. n = 7 (mice). The minimal number of events used in the analysis was 20,000. Groups represent: naïve – unimmunized mice, 2.5 µg s.c. – immunization with 2.5 µg AER subcutaneously, 0.5 µg i.d. – immunization with 0.5 µg AER intradermally, 2.5 µg i.d. – immunization with 2.5 µg AER intradermally.

a bifunctional central memory T-cell subset CD8⁺ IL-2⁺ IFNγ⁺ TNFα⁻ CD44⁻ CD62L⁺ was increased in both the s.c. and i.d. vaccinated groups. No differences in lower and higher AER i.d. vaccinated groups were found. Like for CD4⁺ T cells, also here, although patterns were consistent, there was a substantial spread within the data from the two experiments.

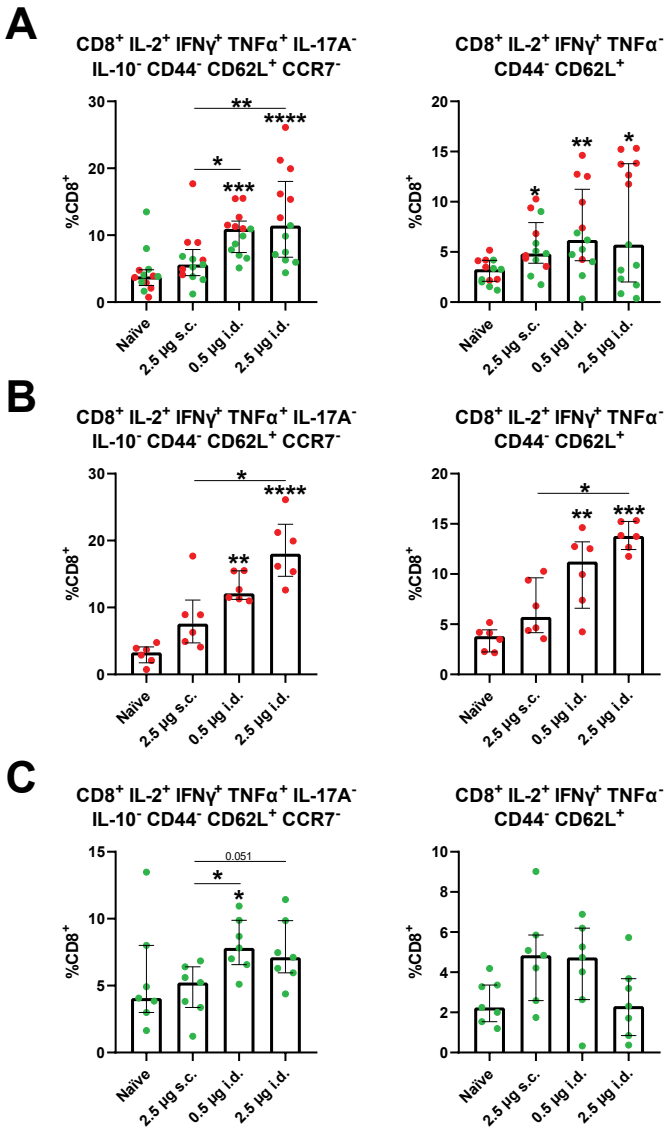

Figure 5. Variations in the abundance of CD8⁺ T-cell populations within restimulated splenocytes from immunized mice. Each graph identifies the markers characterizing the respective populations and displays the percentage values of these populations as median ± IQR within the CD3⁺ CD19⁻ CD4⁻CD8⁺ cell subset. A) Combined results from both experiments. Each dot represents a single mouse, and the results of the same experiment are shown in one color. n = 13 (mice). B) Results from the first experiment. n = 6 (mice). C) Results from the second experiment. n = 7 (mice). The minimal number of events used in the analysis was 20,000. Groups represent: naïve – unimmunized mice, 2.5 µg s.c. – immunization with 2.5 µg AER subcutaneously, 0.5 µg i.d. – immunization with 0.5 µg AER intradermally, 2.5 µg i.d. – immunization with 2.5 µg AER intradermally.

3.3 Differentially abundant AER-specific B-cells from splenocytes ex vivo

B-cells are believed to play a supportive role in immune responses through several mechanisms, including antigen presentation, immune regulation, and antibody production.[40] B-cell data ($CD3^-$ $CD19^+$) were analyzed using the UMAP algorithm for dimensionality reduction and visual assessment of global changes across experimental groups (Figure 6). The UMAP plots revealed subtle differences in the abundance of B-cell subpopulations between the groups. Notably, color-gradient plots indicated that the most pronounced differences were observed in B-cell populations expressing IgM, IgD, and CD69 markers.

To confirm these observations and further investigate the differences, a quantitative analysis was conducted. Differential abundance analysis identified statistically significant B-cell subsets, which were subsequently examined in detail using univariate plots (Figures 7 and 8). Three distinct populations were identified among the AER-restimulated B-cells, all expressing the activation marker CD69 (Figure 7). The predominant population was characterized as $MHCII^+$ IgM^- IgD^- $B220^+$ $CD69^+$ B-cells, indicative of germinal center B-cells. This was followed by $MHCII^+$ IgM^- IgD^+ $B220^+$ $CD69^+$ B-cells, resembling follicular B/B2 cells, and $MHCII^+$ IgM^+ IgD^- $B220^+$ $CD69^+$ B-cells, akin to marginal zone B-cell and transitional 1 B-cells (follicular B/B2). These three B-cell subsets exhibited higher abundance in the groups vaccinated i.d. compared to s.c. We also observed three subsets of B-cells that were $MHCII^-$, expressed B220, and varied in IgM and IgD levels (Figure 8). MHCII is downregulated as B-cells differentiate into antibody-producing B-cells.[41] We can speculate that these cells might be transitional subsets of antibody-producing B-cells. All three subsets were significantly increased in the i.d. but not s.c. groups, suggesting that i.d. immunization led to better B-cell stimulation and, consequently, humoral responses. There were no differences between i.d. vaccinated groups.

To further explore the humoral immune response, AER-specific antibody titers in sera of immunized mice were quantified (Figure 9). Total AER-specific antibody titers in sera from naïve mice were below the detection limit, preventing the assessment of antibody subtypes in these samples. In line with the flow cytometry results, significantly higher total antibody titers in both i.d. groups compared to the s.c. group were observed. Analyzing the antibody subtypes, no difference in IgG1 levels

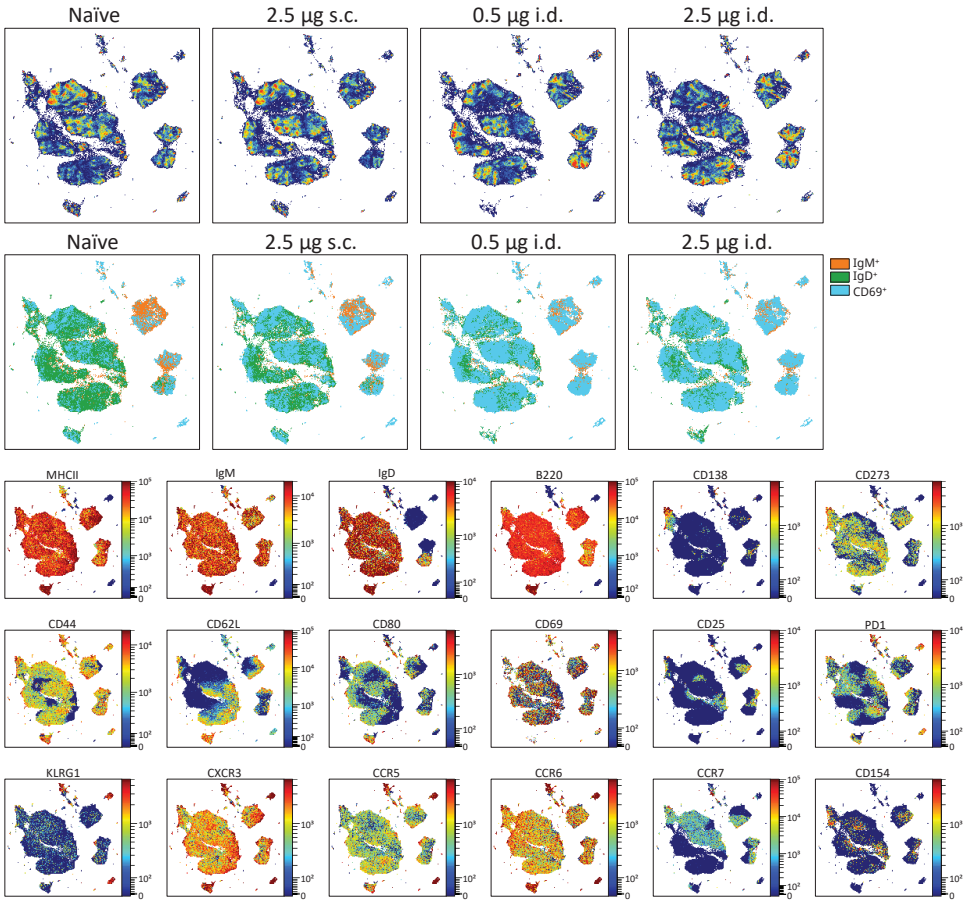

Figure 6. UMAP visualization displays concatenated spleen-derived B-cells ($CD3^-$ $CD19^+$) from all tested mice in each group, highlighting differences in the abundance of various cell populations. This was complemented by color-continuous plots showing the distribution of cellular markers. Groups represent: naïve – unimmunized mice, 2.5 µg s.c. – immunization with 2.5 µg AER subcutaneously, 0.5 µg i.d. – immunization with 0.5 µg AER intradermally, 2.5 µg i.d. – immunization with 2.5 µg AER intradermally.

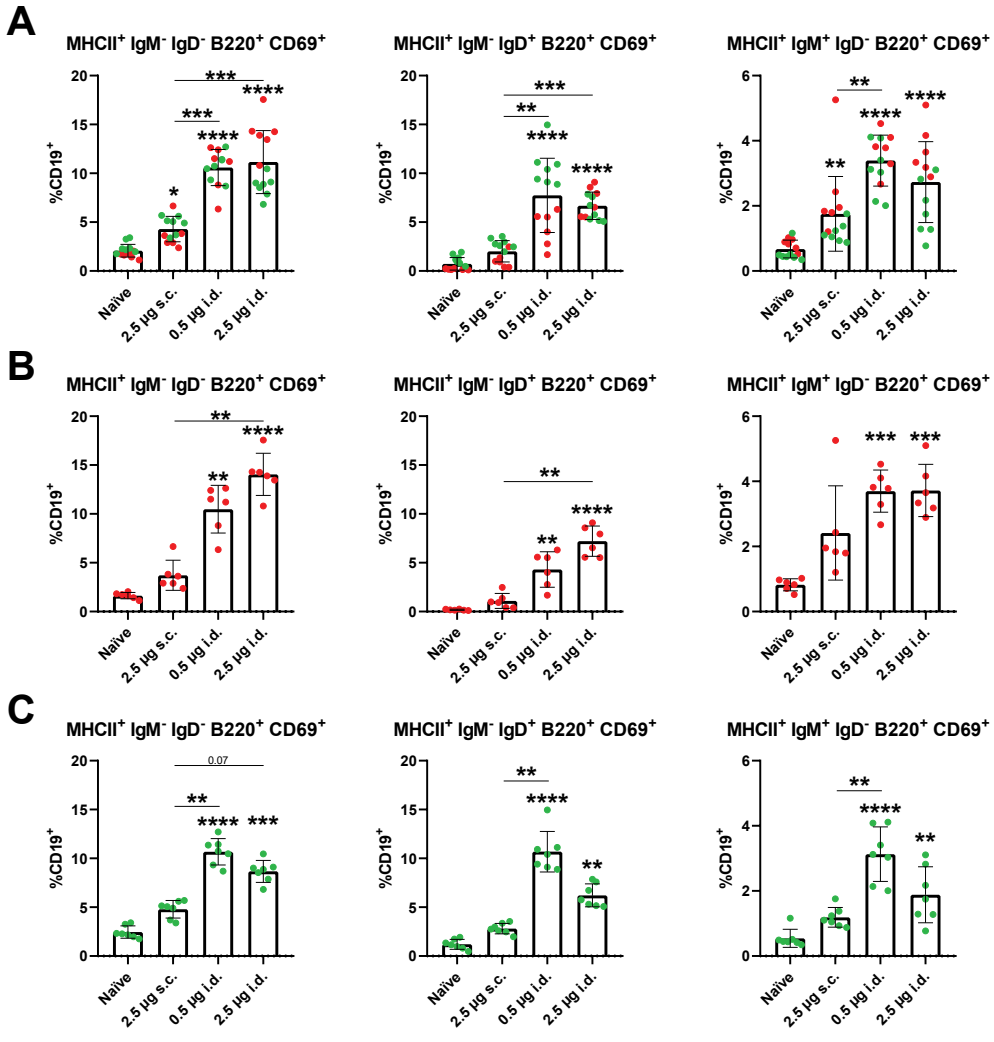

Figure 7. Differentially abundant populations of $CD3^{-}$ $CD19^{+}$ B-cells expressing CD69 in restimulated splenocytes from immunized mice. The markers defining each population are specified above the respective graphs, which present the percentages of these populations as median ± IQR within the overall cell subset. A) Combined results from both experiments. Each dot represents a single mouse, and the results of the same experiment are shown in one color. n = 13 (mice). B) Results from the first experiment. n = 6 (mice). C) Results from the second experiment. n = 7 (mice). The minimal number of events used in the analysis was 20,000. Groups represent: naïve – unimmunized mice, 2.5 µg s.c. – immunization with 2.5 µg AER subcutaneously, 0.5 µg i.d. – immunization with 0.5 µg AER intradermally, 2.5 µg i.d. – immunization with 2.5 µg AER intradermally.

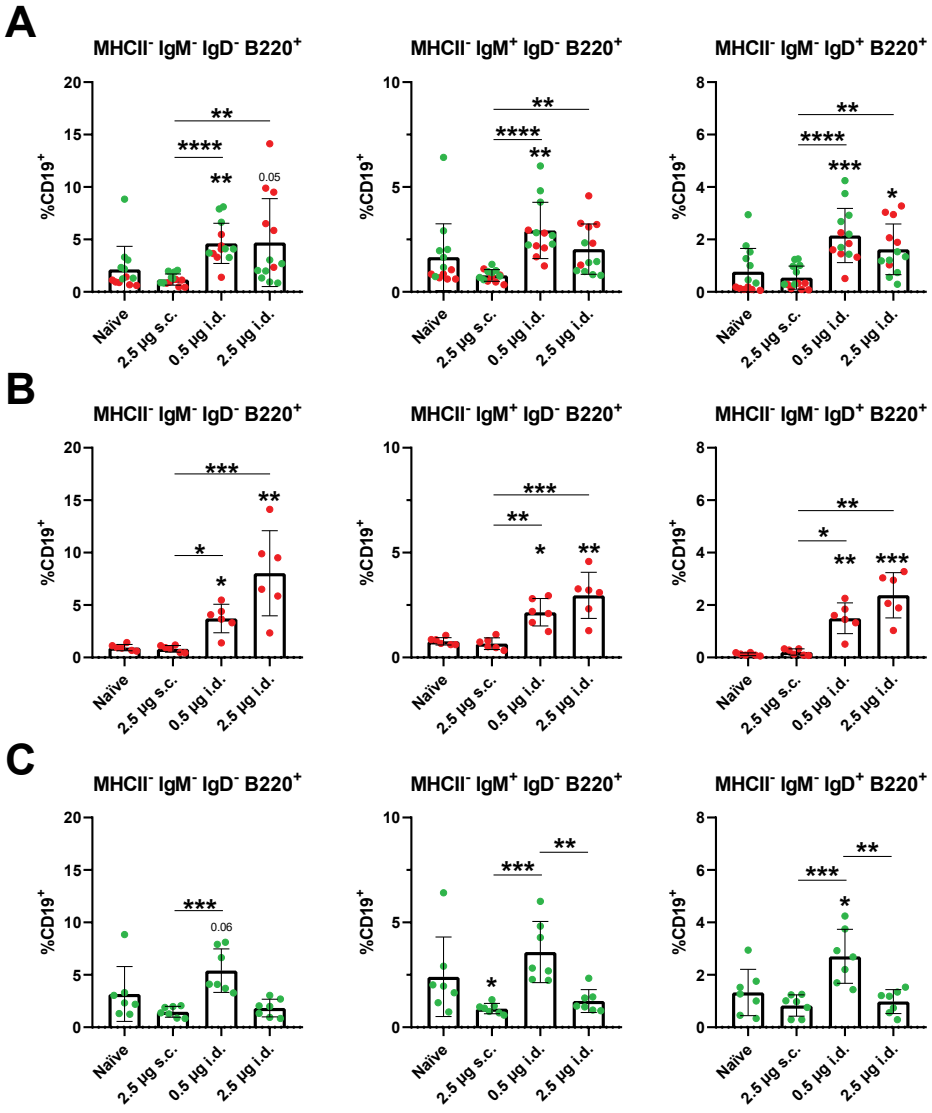

Figure 8. Differentially abundant populations of CD3⁻ CD19⁺ B-cells in restimulated splenocytes from immunized mice. The markers defining each population are specified above the respective graphs, which present the percentages of these populations as median ± IQR within the overall cell subset. A) Combined results from both experiments. Each dot represents a single mouse, and the results of the same experiment are shown in one color. n = 13 (mice). B) Results from the first experiment. n = 6 (mice). C) Results from the second experiment. n = 7 (mice). The minimal number of events used in the analysis was 20,000. Groups represent: naïve – unimmunized mice, 2.5 µg s.c. – immunization with 2.5 µg AER subcutaneously, 0.5 µg i.d. – immunization with 0.5 µg AER intradermally, 2.5 µg i.d. – immunization with 2.5 µg AER intradermally.

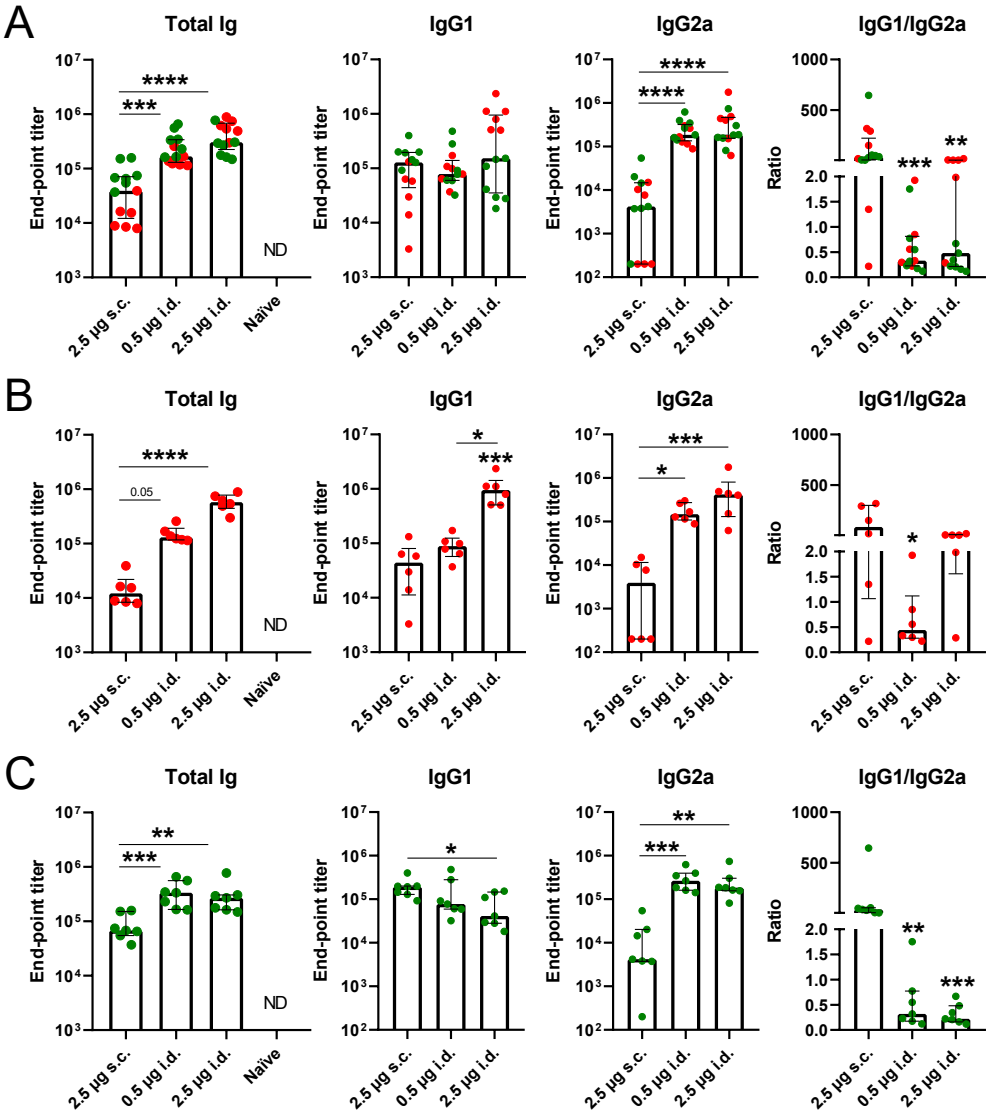

Figure 9. Quantification of AER-specific serum antibodies. The type of antibody measured is indicated above each graph. Values represent end-point titers. A) Combined results from both experiments. Each dot represents a single mouse, and the results of the same experiment are shown in one color. n = 13 (mice). B) Results from the first experiment. n = 6 (mice). C) Results from the second experiment. n = 7 (mice). Groups represent: 2.5 µg s.c. – immunization with 2.5 µg AER subcutaneously, 0.5 µg i.d. – immunization with 0.5 µg AER intradermally, 2.5 µg i.d. – immunization with 2.5 µg AER intradermally, naïve – unimmunized mice.

was detectable; however, IgG2a titers were significantly increased in i.d. groups. These findings might be indicative of overall dominant T-helper responses. Increased IgG2 levels are related to more robust Th1-like immunity, while higher IgG1 levels compared to IgG2 can be linked to Th2-like responses. This shift in T-helper response balance is reflected in the IgG1/IgG2a ratio. However, no increased Th2 subsets were identified in the spectral flow cytometry data in the s.c. group. The Ig ratio in s.c. group is possibly related to suboptimal IFNγ production that led to less efficient antibody class switching. The antibody titters were very similar in lower and higher AER groups vaccinated i.d.

4. DISCUSSION

TB continues to be a global health challenge, particularly in economically disadvantaged and marginalized populations.[1] Innovations in vaccine technology, such as subunit vaccines and biocompatible NP-based vaccine delivery systems, offer promise for safer, more effective immunization strategies.[7] This includes exploring i.d. vaccination routes. I.d. vaccination offers several benefits over traditional methods by delivering vaccines into the skin's dermis, which is rich in APCs.[19,20] This approach often leads to robust immune responses with smaller doses, which is crucial for expanding accessibility, especially in middle- and low-income countries as well as dose sparing.[21–24] Reduced vaccine dosages lower costs, and the shorter needles used with this method reduce discomfort, potentially improving patient compliance and better vaccination coverage.[25] Novel technologies such as microneedle patches may allow for self-administration, which could simplify vaccination efforts. Solid vaccine formulation may potentially improve stability during storage and shelf-life as well as allow for storage at room temperatures. I.d. vaccination emerges as an efficient, cost-effective, and safe strategy that may lead to improved global public health outcomes. This work compared the immunological effects of i.d. administration of low-dose lipid-PLGA hybrid NP-based TB vaccine to the conventional s.c. route.

$CD4^+$ T-cells, especially Th1 cells, are essential in host defence against Mtb through their cytokine production and facilitation of immune responses.[38,39] A key cytokine, IFNγ, plays a significant role in activating macrophages, differentiating $CD8^+$ T-cells, and stimulating B-cells.[42] Concurrently, TNFα synergizes with IFNγ to enhance the production of reactive oxygen and nitrogen species in macrophages, support the migration of immune cells, and facilitate granuloma formation.[43] Comparing the

two routes of administration, both significantly increased the magnitude of IFNγ-producing $CD4^+$ T-cells. However, only i.d. immunizations induced polyfunctional $CD4^+$ T-cells expressing IL-2, IFNγ, and TNFα. In our previous studies,[31,35] AER-based vaccines (at an 8 μg AER dose) formulated with liposomes composed of DOPC:DOPE:DOBAQ:EPC in a 3:5:2:4 ratio (the same lipid ratio used in this study for hybrid NPs), PLGA NPs, and lipid-PLGA hybrid NPs induced high levels of polyfunctional $CD4^+$ T-cells. Coincidentally, these vaccines provided protection against intranasal challenge with live H37Rv Mtb, as evidenced by a significant and immunologically relevant reduction in Mtb bacterial burden in the lungs and spleens of the challenged mice. Other studies in mice[44,45] and humans[46] suggest that these polyfunctional $CD4^+$ T-cells play a crucial and superior role in vaccine induced immunity against Mtb. Nevertheless, some studies challenged this hypothesis.[47,48] In contrast, s.c. immunization induced single positive IL-2-producing T-cells. These results indicate that i.d. immunization induced favorable and protection-associated T-cell subsets, whereas s.c. did not.

The role of cytotoxic $CD8^+$ T-cells in protection against Mtb remains debated. Besides directly eliminating infected cells, these cells also produce cytokines, influence the immune response, and enhance the function of Th1 cells.[49] Studies suggest $CD8^+$ T-cells and Th1 cells are promising targets for new TB vaccines.[38,50] Experiments in mice[51] and non-human primates[52] demonstrate that depletion of $CD8^+$ T-cells increases vulnerability to TB, highlighting their necessity for optimal control of infection, and underscores their vital role during the chronic infection stages.[53] In this study, two differentially abundant $CD8^+$ T-cell subsets were found. The abundance of polyfunctional $CD8^+$ T-cells was increased only in i.d. immunized mice, similarly to the $CD4^+$ counterpart. In our previous work,[31,35] the abundance of polyfunctional CD8+ T-cells was significantly increased, potentially contributing to the observed protection against Mtb infection. Less abundant double-positive IL-2- and IFNγ-producing CD8+ T-cells were increased using both methods.

All the differentially abundant T-cells were found to express CD62L without expressing CD44 or CCR7, indicating they could be a unique subset of central memory T-cells that have lost CD44[54] or could consist of transitional subsets. T-cells with such a profile were shown to offer beneficial anti-Mtb responses, displayed considerable expansion, and provided substantial protection when transferred into $Rag^{-/-}$ mice infected with aerosolized Mtb H37Rv, in contrast to the $CD4^+$ $CD44^{hi}$ $CD62L^{lo}$ cells.[55]

The $CD4^{+}$ $CD44^{lo}$ $CD62L^{hi}$ cells may be an important reservoir of memory cells, potentially offering protection in a manner aligned with the characteristics of central memory T-cells.[55]

Though complex and not fully understood, the role of B-cell and antibody responses in TB immunity is increasingly acknowledged.[56,57] B-cells may contribute to protective immune responses against TB through mechanisms like cytokine release, antigen presentation, immune regulation, opsonization, and direct neutralization of Mtb.[40] Support for their involvement comes from the observation of increased B-cell numbers in infected tissues across species,[58,59] worsened TB susceptibility in B-cell-depleted models reversed by B-cell reintroduction,[60,61] and the normalization of B-cell function after TB treatment.[57] Despite this, some studies using genetic knockouts[62–64] and different infection models[65–67] have questioned their significance in TB immunity. Therefore, the B-cell arm of immune responses was also investigated in this study. Six differentially abundant B-cell subsets were identified, of which three expressed CD69 activation marker. In all six identified subsets, i.d. immunized groups showed a significantly higher abundance of B-cells compared to the s.c. route, indicating that the B-cell arm of immunity was better activated by i.d. immunization.

Antibodies are also postulated to offer protection against TB, evidenced e.g. by successful serum therapy in immunodeficient mice[68] and reduced Mtb load through high-dose immunoglobulin treatments.[69] Protective effects were further demonstrated through serum transfers from latently infected patients and exposure-resistant individuals,[70] as well as monoclonal antibodies targeting specific mycobacterial antigens, which improved survival, limited spread, reduced tissue damage, and lowered bacterial counts.[71–76] In this study, significant total AER-specific antibody responses were observed in all immunized mice, though i.d. immunization induced significantly higher titers compared to s.c. route. Antibody subtype analysis revealed that AER-specific IgG1 titers were similar in all immunized mice; however, IgG2a titers were significantly higher in both lower and higher AER dose i.d. immunized groups compared to the s.c. one. Moreover, in four out of thirteen mice in the s.c. group, IgG2a titers were below the detection level, indicating suboptimal antibody class switching in these mice.

The results from all of the evaluated cellular and humoral immune responses indicated that i.d. immunization provided superior outcomes compared to s.c. immunization. This finding is in line with previously published research demonstrating that i.d. immunization provides the same or improved immune responses to vaccines.[22,23,77,78] Future research will evaluate the effectiveness of these vaccines in Mtb challenge studies.

5. CONCLUSIONS

This study assessed the immunogenicity of a novel subunit TB vaccine, focusing on the impact of different immunization routes. The vaccine formulation included the Ag85B-ESAT6-Rv2034 fusion antigen, adjuvants CpG and MPLA, and a cationic lipid (DOPC:DOPE:DOBAQ:EPC in a 3:5:2:4 ratio) combined with PLGA in a hybrid nanoparticle delivery system. *In vivo* experiments revealed that the vaccine elicited enhanced T-cell responses across both immunization routes. Notably, mice immunized via the i.d. route exhibited significant increases in polyfunctional $CD4^+$ and $CD8^+$ T-cell responses compared to the s.c. one, which are considered crucial for protection against Mtb. In contrast, s.c. administration resulted in increased monofunctional (IL-2-producing) T-cells and no polyfunctional responses. Also, the i.d. route led to a rise in $CD69^+$ B-cell subpopulations, which were higher compared to s.c. vaccinated mice. While both immunization routes increased antigen-specific antibody titers, the i.d. route resulted in markedly higher total Ig and IgG2a titers compared to the s.c. route. The comprehensive analysis of cellular and humoral responses indicates that i.d. immunization is superior to s.c. immunization. These results provide insights into the differential effects of vaccine administration routes and underscore the potential of the tested vaccine as a promising candidate for further TB vaccine development. Further research, including Mtb challenge studies, is necessary to confirm the efficacy of this vaccine approach.

ABBREVIATIONS

AER, Ag85B-ESAT6-Rv2034 antigen; APC, antigen-presenting cell; Ag, antigen(-adjuvant mix group); BCG, Mycobacterium bovis Bacillus Calmette–Guérin; CCR, C-C chemokine receptor type; CD, cluster of differentiation; CpG ODN, cytosine-phosphorothioate-guanine oligodeoxynucleotides; CXCR, C-X-C motif chemokine receptor; DC, dendritic cell; DOBAQ, N-(4-carboxybenzyl)-N,N-dimethyl-2,3-bis(oleoyloxy)propan-1-aminium; DOPC, 1,2-dioleoyl-sn-glycero-3-phosphocholine;

DOPE, 1,2-dioleoyl-sn-glycero-3-phosphoethanolamine; EPC, 1,2-dioleoyl-sn-glycero-3-ethylphosphocholine; FBS, fetal bovine serum; FDR, false discovery rate; HLA, human leukocyte antigen; HRP, horse radish peroxide; IFN, interferon; Ig, immunoglobulin, IL, interleukin; i.d., intradermal; IQR, interquartile range; KLRG1, killer cell lectin-like receptor subfamily G member 1; LUMC, Leiden University Medical Center; MDR-TB, multidrug-resistant tuberculosis; MHC, major histocompatibility complex; MPLA, monophosphoryl lipid A; Mtb, *Mycobacterium tuberculosis*; NP, nanoparticle; PCR, polymerase chain reaction; PD-1, programmed cell death protein 1; PDI, polydispersity index; PE, phosphatidylethanolamine; pH, pH-sensitive liposome group; PLGA, poly(D,L-lactic-co-glycolic acid); rpm, rounds per minute; s.c., subcutaneous; TB, tuberculosis; Th1/Th2, type 1/2 helper T-cell; TLR, Toll-like receptor; TNF, tumor necrosis factor; UMAP, uniform manifold approximation and projection.

FUNDING

This work was supported by the Dutch Research Council (NWO) Domain Applied and Engineering Sciences grant, project number: 15240.

CREDIT AUTHOR STATEMENT

M.M. Szachniewicz: Conceptualization, Methodology, Formal Analysis, Investigation, Writing – Original Draft. **S.J.F. van den Eeden**: Conceptualization, Methodology, Investigation, Writing – Original Draft. **K.E. van Meijgaarden**: Conceptualization, Methodology, Writing – Review & Editing, Supervision. **K.L.M.C. Franken**: Methodology, Investigation, Resources. **S. van Veen**: Methodology, Formal Analysis. **A. Geluk**: Conceptualization, Writing – Review & Editing, Project Administration, Funding Acquisition, Supervision. **J.A. Bouwstra**: Conceptualization, Writing – Review & Editing, Project Administration, Funding Acquisition, Supervision. **T.H.M. Ottenhoff**: Conceptualization, Writing – Review & Editing, Project Administration, Funding Acquisition, Primary supervision.

DECLARATIONS OF INTEREST

None.

REFERENCES

1. Bloom, B. R. A half-century of research on tuberculosis: Successes and challenges. *Journal of Experimental Medicine* 220, (2023).
2. Schrager, L. K. *et al.* The status of tuberculosis vaccine development. *Lancet Infectious Diseases* 20, e28–e37 (2020).
3. World Health Organization. *Global Tuberculosis Report 2023*. (2023).
4. Brewer, T. F. Preventing Tuberculosis with Bacillus Calmette-Guérin Vaccine: A Meta-Analysis of the Literature. *Clinical Infectious Diseases* 31, S64–S67 (2000).
5. Trunz, B. B. *et al.* Effect of BCG vaccination on childhood tuberculous meningitis and miliary tuberculosis worldwide: a meta-analysis and assessment of cost-effectiveness. *Lancet* 367, 1173–1180 (2006).
6. Moyle, P. M. & Toth, I. Modern Subunit Vaccines: Development, Components, and Research Opportunities. *ChemMedChem* 8, 360–376 (2013).
7. Christensen, D. *et al.* Cationic liposomes as vaccine adjuvants. *Expert Review of Vaccines* 10, 513–521 (2011).
8. Alsaab, H. O. *et al.* PLGA-Based Nanomedicine: History of Advancement and Development in Clinical Applications of Multiple Diseases. *Pharmaceutics* 14, 2728 (2022).
9. Khademi, F. *et al.* Induction of strong immune response against a multicomponent antigen of Mycobacterium tuberculosis in BALB/c mice using PLGA and DOTAP adjuvant. *APMIS* 126, 509–514 (2018).
10. Khademi, F. *et al.* A novel antigen of Mycobacterium tuberculosis and MPLA adjuvant co-entrapped into PLGA:DDA hybrid nanoparticles stimulates mucosal and systemic immunity. *Microbial Pathogenesis* 125, 507–513 (2018).
11. Moon, J. J. *et al.* Antigen-Displaying Lipid-Enveloped PLGA Nanoparticles as Delivery Agents for a Plasmodium vivax Malaria Vaccine. *PLoS One* 7, e31472 (2012).
12. Liu, L. *et al.* Hyaluronic Acid-Modified Cationic Lipid-PLGA Hybrid Nanoparticles as a Nanovaccine Induce Robust Humoral and Cellular Immune Responses. *ACS Applied Materials & Interfaces* 8, 11969–11979 (2016).
13. Liu, L. *et al.* Immune responses to vaccines delivered by encapsulation into and/or adsorption onto cationic lipid-PLGA hybrid nanoparticles. *Journal of Controlled Release* 225, 230–239 (2016).

14. Hadinoto, K. *et al.* Lipid–polymer hybrid nanoparticles as a new generation therapeutic delivery platform: A review. *European Journal of Pharmaceutics and Biopharmaceutics* 85, 427–443 (2013).
15. Sah, H. *et al.* Concepts and practices used to develop functional PLGA-based nanoparticulate systems. *International Journal of Nanomedicine* 8, 747–765 (2013).
16. Pandita, D. *et al.* Hybrid poly(lactic-co-glycolic acid) nanoparticles: design and delivery prospectives. *Drug Discovery Today* 20, 95–104 (2015).
17. Ghitman, J. *et al.* Review of hybrid PLGA nanoparticles: Future of smart drug delivery and theranostics medicine. *Materials & Design* 193, 108805 (2020).
18. Rose, F. *et al.* A strong adjuvant based on glycol-chitosan-coated lipid-polymer hybrid nanoparticles potentiates mucosal immune responses against the recombinant Chlamydia trachomatis fusion antigen CTH522. *Journal of Controlled Release* 271, 88–97 (2018).
19. Kashem, S. W. *et al.* Antigen-Presenting Cells in the Skin. *Annual Review of Immunology* 35, 469–499 (2017).
20. Levin, C. *et al.* Tailored immunity by skin antigen-presenting cells. *Human Vaccines & Immunotherapeutics* 11, 27–36 (2015).
21. Fabrizi, F. *et al.* Meta-analysis: intradermal vs. intramuscular vaccination against hepatitis B virus in patients with chronic kidney disease. *Alimentary Pharmacology & Therapeutics* 24, 497–506 (2006).
22. Schnyder, J. L. *et al.* Fractional dose of intradermal compared to intramuscular and subcutaneous vaccination - A systematic review and meta-analysis. *Travel Medicine and Infectious Disease* 37, 101868 (2020).
23. Schnyder, J. L. *et al.* Comparison of equivalent fractional vaccine doses delivered by intradermal and intramuscular or subcutaneous routes: A systematic review. *Travel Medicine and Infectious Disease* 41, 102007 (2021).
24. Egunsola, O. *et al.* Immunogenicity and Safety of Reduced-Dose Intradermal vs Intramuscular Influenza Vaccines: A Systematic Review and Meta-analysis. *JAMA Network Open* 4, e2035693–e2035693 (2021).
25. Witting, N. *et al.* Intramuscular and intradermal injection of capsaicin: a comparison of local and referred pain. *Pain* 84, 407–412 (2000).
26. Karbalaei Zadeh Babaki, M. *et al.* Antigen 85 complex as a powerful Mycobacterium tuberculosis immunogene: Biology, immune-pathogenicity, applications in diagnosis, and vaccine design. *Microbial Pathogenesis* 112, 20–29 (2017).

27. Li, W. *et al.* A recombinant adenovirus expressing CFP10, ESAT6, Ag85A and Ag85B of Mycobacterium tuberculosis elicits strong antigen-specific immune responses in mice. *Molecular Immunology* 62, 86–95 (2014).
28. You, Q. *et al.* Subcutaneous Administration of Modified Vaccinia Virus Ankara Expressing an Ag85B-ESAT6 Fusion Protein, but Not an Adenovirus-Based Vaccine, Protects Mice Against Intravenous Challenge with Mycobacterium tuberculosis. *Scandinavian Journal of Immunology* 75, 77–84 (2012).
29. Commandeur, S. *et al.* An Unbiased Genome-Wide Mycobacterium tuberculosis Gene Expression Approach To Discover Antigens Targeted by Human T Cells Expressed during Pulmonary Infection. *The Journal of Immunology* 190, 1659–1671 (2013).
30. Franken, K. L. M. C. *et al.* Purification of His-Tagged Proteins by Immobilized Chelate Affinity Chromatography: The Benefits from the Use of Organic Solvent. *Protein Expression and Purification* 18, 95–99 (2000).
31. Szachniewicz, M. M. *et al.* Evaluation of PLGA, lipid-PLGA hybrid nanoparticles, and cationic pH-sensitive liposomes as tuberculosis vaccine delivery systems in a Mycobacterium tuberculosis challenge mouse model – A comparison. *International Journal of Pharmaceutics* 666, 124842 (2024).
32. Szachniewicz, M. M. *et al.* Cationic pH-sensitive liposomes as tuberculosis subunit vaccine delivery systems: Effect of liposome composition on cellular innate immune responses. *International Immunopharmacology* 145, 113782 (2025).
33. Szachniewicz, M. M. *et al.* Intrinsic immunogenicity of liposomes for tuberculosis vaccines: Effect of cationic lipid and cholesterol. *European Journal of Pharmaceutical Sciences* 195, 106730 (2024).
34. Geluk, A. *et al.* A multistage-polyepitope vaccine protects against Mycobacterium tuberculosis infection in HLA-DR3 transgenic mice. *Vaccine* 30, 7513–7521 (2012).
35. Szachniewicz, M. M. *et al.* Cationic pH-sensitive liposome-based subunit tuberculosis vaccine induces protection in mice challenged with Mycobacterium tuberculosis. *European Journal of Pharmaceutics and Biopharmaceutics* 203, 114437 (2024).
36. R Core Team. R: A language and environment for statistical computing, (2023).
37. RStudio Team. RStudio: Integrated Development Environment for R, (2023).
38. Ottenhoff, T. H. M. & Kaufmann, S. H. E. Vaccines against Tuberculosis: Where Are We and Where Do We Need to Go? *PLoS Pathogens* 8, e1002607 (2012).

39. Ottenhoff, T. H. M. *et al.* Human CD4 and CD8 T Cell Responses to Mycobacterium tuberculosis: Antigen Specificity, Function, Implications and Applications. *Handbook of Tuberculosis* 119–155 (2008.
40. Rijnink, W. F. *et al.* B-Cells and Antibodies as Contributors to Effector Immune Responses in Tuberculosis. *Frontiers in Immunology* 12, 640168 (2021).
41. Giles, J. R. *et al.* B Cell–Specific MHC Class II Deletion Reveals Multiple Nonredundant Roles for B Cell Antigen Presentation in Murine Lupus. *The Journal of Immunology* 195, 2571–2579 (2015).
42. Prezzemolo, T. *et al.* Functional signatures of human CD4 and CD8 T cell responses to Mycobacterium tuberculosis. *Frontiers in Immunology* 5, 83298 (2014).
43. Cavalcanti, Y. V. N. *et al.* Role of TNF-alpha, IFN-gamma, and IL-10 in the development of pulmonary tuberculosis. *Pulmonary Medicine* 2012:1, 745483 (2012).
44. Aagaard, C. *et al.* A multistage tuberculosis vaccine that confers efficient protection before and after exposure. *Nature Medicine* 17:2, 189–194 (2011).
45. Lindenstrøm, T. *et al.* Tuberculosis Subunit Vaccination Provides Long-Term Protective Immunity Characterized by Multifunctional CD4 Memory T Cells. *The Journal of Immunology* 182, 8047–8055 (2009).
46. Abel, B. *et al.* The Novel Tuberculosis Vaccine, AERAS-402, Induces Robust and Polyfunctional CD4+ and CD8+ T Cells in Adults. *American Journal of Respiratory and Critical Care Medicine* 181, 1407–1417 (2012).
47. Harari, A. *et al.* Dominant TNF-α+ Mycobacterium tuberculosis–specific CD4+ T cell responses discriminate between latent infection and active disease. *Nature Medicine* 17:3, 372–376 (2011).
48. Lewinsohn, D. A., Lewinsohn, D. M. & Scriba, T. J. Polyfunctional CD4+ T cells as targets for tuberculosis vaccination. *Frontiers in Immunology* 8, 295382 (2017).
49. Lu, Y. J. *et al.* CD4 T cell help prevents CD8 T cell exhaustion and promotes control of Mycobacterium tuberculosis infection. *Cell Reports* 36, 109696 (2021).
50. Boom, W. H. New TB vaccines: is there a requirement for CD8+ T cells? *Journal of Clinical Investigation* 117, 2092–2094 (2007).
51. Woodworth, J. S. *et al.* Mycobacterium tuberculosis-Specific CD8+ T Cells Require Perforin to Kill Target Cells and Provide Protection In Vivo. *The Journal of Immunology* 181, 8595–8603 (2008).

52. Lin, P. L. *et al.* CD4 T Cell Depletion Exacerbates Acute Mycobacterium tuberculosis While Reactivation of Latent Infection Is Dependent on Severity of Tissue Depletion in Cynomolgus Macaques. *AIDS Research and Human Retroviruses* 28, 1693–1702 (2012).
53. Van Pinxteren, L. A. H. *et al.* Control of latent Mycobacterium tuberculosis infection is dependent on CD8 T cells. *European Journal of Immunology* 30, 3689–3698 (2000).
54. Henao-Tamayo, M. I. *et al.* Phenotypic definition of effector and memory T-lymphocyte subsets in mice chronically infected with mycobacterium tuberculosis. *Clinical and Vaccine Immunology* 17, 618–625 (2010).
55. Kipnis, A. *et al.* Memory T Lymphocytes Generated by Mycobacterium bovis BCG Vaccination Reside within a CD4 CD44lo CD62 Ligandhi Population. *Infection and Immunity* 73, 7759 (2005).
56. Duong, V. T. *et al.* Towards the development of subunit vaccines against tuberculosis: The key role of adjuvant. *Tuberculosis* 139, 102307 (2023).
57. Joosten, S. A. *et al.* Patients with Tuberculosis Have a Dysfunctional Circulating B-Cell Compartment, Which Normalizes following Successful Treatment. *PLoS Pathogens* 12, e1005687 (2016).
58. Phuah, J. Y. *et al.* Activated B Cells in the Granulomas of Nonhuman Primates Infected with Mycobacterium tuberculosis. *American Journal of Pathology* 181, 508–514 (2012).
59. Tsai, M. C. *et al.* Characterization of the tuberculous granuloma in murine and human lungs: cellular composition and relative tissue oxygen tension. *Cell Microbiology* 8, 218–232 (2006).
60. Maglione, P. J. *et al.* B Cells Moderate Inflammatory Progression and Enhance Bacterial Containment upon Pulmonary Challenge with Mycobacterium tuberculosis. *The Journal of Immunology* 178, 7222–7234 (2007).
61. Phuah, J. *et al.* Effects of B cell depletion on early Mycobacterium tuberculosis infection in cynomolgus macaques. *Infection and Immunity* 84, 1301–1311 (2016).
62. Khera, A. K. *et al.* Role of B Cells in Mucosal Vaccine–Induced Protective CD8+ T Cell Immunity against Pulmonary Tuberculosis. *The Journal of Immunology* 195, 2900–2907 (2015).
63. Torrado, E. *et al.* Differential and Site Specific Impact of B Cells in the Protective Immune Response to Mycobacterium tuberculosis in the Mouse. *PLoS One* 8, e61681 (2013).

64. Vordermeier, H. M. *et al.* Increase of tuberculous infection in the organs of B cell-deficient mice. *Clinical & Experimental Immunology* 106, 312–316 (2003).
65. Turner, J. *et al.* The progression of chronic tuberculosis in the mouse does not require the participation of B lymphocytes or interleukin-4. *Experimental Gerontology* 36, 537–545 (2001).
66. Bosio, C. M. *et al.* Infection of B Cell-Deficient Mice with CDC 1551, a Clinical Isolate of Mycobacterium tuberculosis: Delay in Dissemination and Development of Lung Pathology. *The Journal of Immunology* 164, 6417–6425 (2000).
67. Johnson, C. M. *et al.* Mycobacterium tuberculosis aerogenic rechallenge infections in B cell-deficient mice. *Tubercle and Lung Disease* 78, 257–261 (1997).
68. Guirado, E. *et al.* Passive serum therapy with polyclonal antibodies against Mycobacterium tuberculosis protects against post-chemotherapy relapse of tuberculosis infection in SCID mice. *Microbes and Infection* 8, 1252–1259 (2006).
69. Roy, E. *et al.* Therapeutic efficacy of high-dose intravenous immunoglobulin in Mycobacterium tuberculosis infection in mice. *Infection and Immunity* 73, 6101–6109 (2005).
70. Li, H. *et al.* Latently and uninfected healthcare workers exposed to TB make protective antibodies against Mycobacterium tuberculosis. *Proceedings of the National Academy of Sciences of the United States of America* 114, 5023–5028 (2017).
71. Zimmermann, N. *et al.* Human isotype-dependent inhibitory antibody responses against Mycobacterium tuberculosis. *EMBO Molecular Medicine* 8, 1325–1339 (2016).
72. Balu, S. *et al.* A Novel Human IgA Monoclonal Antibody Protects against Tuberculosis. *The Journal of Immunology* 186, 3113–3119 (2011).
73. Lu, L. L. *et al.* A Functional Role for Antibodies in Tuberculosis. *Cell* 167, 433-443. e14 (2016).
74. Davies, L. R. L. *et al.* Age and sex influence antibody profiles associated with tuberculosis progression. *Nature Microbiology* 9:6, 1513-1525 (2024).
75. Grace, P. S. *et al.* Antibody Subclass and Glycosylation Shift Following Effective TB Treatment. *Frontiers in Immunology* 12, 679973 (2021).
76. Alter, G. *et al.* Antibody glycosylation in inflammation, disease and vaccination. *Seminars in Immunology* 39, 102–110 (2018).

77. Leone, M. *et al.* Hyaluronan-based dissolving microneedles with high antigen content for intradermal vaccination: Formulation, physicochemical characterization and immunogenicity assessment. *European Journal of Pharmaceutics and Biopharmaceutics* 134, 49–59 (2019).
78. Ogai, N. *et al.* Enhanced immunity in intradermal vaccination by novel hollow microneedles. *Skin Research and Technology* 24, 630–635 (2018).